

Design and performance of an R- θ fiber positioner for the BigBOSS instrument

Joseph H. Silber¹, Christoph Schenk¹, Eric Anderssen¹, Chris Bebek¹, Frederic Becker¹, Robert Besuner², Mario Cepeda¹, Jerry Edelstein², Henry Heetderks², Patrick Jelinsky¹, Thomas Johnson¹, Armin Karcher¹, Paul Perry¹, Rodney Post¹, Michael Sholl², Kenneth Wilson¹, Zengxiang Zhou¹

¹Lawrence Berkeley National Laboratory, Berkeley CA

²University of California at Berkeley Space Sciences Laboratory, Berkeley CA

ABSTRACT

The BigBOSS instrument is a proposed multi-object spectrograph for the Mayall 4m telescope at Kitt Peak, which will measure the redshift of 20 million galaxies and map the expansion history of the universe over the past 8 billion years, surveying 10-20 times the volume of existing studies. For each 20 minute observation, 5000 optical fibers are individually positioned by a close-packed array of 5000 robotic positioner mechanisms. Key mechanical constraints on the positioners are: \varnothing 12mm hardware envelope, \varnothing 14mm overlapping patrol zones, open-loop targeting accuracy $\leq 40\mu\text{m}$, and step resolution $\leq 5\mu\text{m}$, among other requirements on envelope, power, stability, and speed. This paper describes the design and performance of a newly-developed fiber positioner with R- θ polar kinematics, in which a flexure-based linear R-axis is stacked on a rotational θ -axis. Benefits over the usual eccentric parallel axis θ - ϕ kinematic approach include faster repositioning, simplified anti-collision schemes, and inherent anti-backlash preload. Performance results are given for complete positioner assemblies as well as sub-component hardware characterization.

Keywords: Optical fiber positioner, BigBOSS, flexure kinematics, fiber fed spectrograph, miniature actuator

Contact: jhsilber@lbl.gov

1. INTRODUCTION

The BigBOSS instrument includes a new prime focus corrector, focal plate with 5000 robotic fiber positioners, an optical fiber system[1], and an array of spectrographs[2]. The corrector focuses galaxy images from the Mayall primary mirror onto a virtual focal surface composed of 5000 optical fibers. These are remotely repositioned to new targets for each observation, and the collected light is then transmitted off the telescope to the multi-object spectrograph.

Unique challenges to the design of the robotic fiber positioners flow down from science requirements, discussed by Schlegel et al. [3][4] and by Mostek et al. [5].

The primary requirements can be summarized as:

- Size: \varnothing 12mm (for 12mm center-center pitch)
- Alignment: $< 0.15^\circ$ tilt error
- Axial location: $< 5\mu\text{m}$
- Axial motion: $< 20\mu\text{m}$ defocus over range of motion
- Accuracy: $< 40\mu\text{m}$
- Resolution: $< 5\mu\text{m}$
- Speed: $< 45\text{sec}$ total repositioning time
- Lifetime: $> 20\text{k}$ repositioning cycles

along with secondary requirements on power, cooling, lifetime, and service interfaces.

Various fiber positioner designs have been produced for other multi-object spectrographs, including LAMOST [6] and FMOS [7] (the Echidna positioner). These have fallen into three categories:

- Stepper-driven θ - ϕ , in the $\varnothing 25\text{mm}$ size class (e.g. LAMOST, SIDE [8])
- Piezo-driven tip-tilt spine (e.g. Echidna)
- Piezo-driven θ - ϕ , in the $\varnothing 8\text{mm}$ size class (e.g. Cobra [9])

To achieve BigBOSS' fiber density at the focal surface, a 4x reduction in cross-section is necessary from the class of $\varnothing 25\text{mm}$ positioners which has been previously demonstrated for LAMOST and SIDE. Those positioners have " θ - ϕ " kinematics (discussed below), which incurs control complexity and repositioning delay for the anti-collision schemes between adjacent positioners (which must patrol in overlapping envelopes, as shown in Figure 1). The tip-tilt type kinematics of Echidna greatly exceeds the allowable tilt error (0.15°) for BigBOSS, and piezo-driven positioners such as Cobra have inherent control and repeatability challenges, which are compounded by the anti-collision challenge.

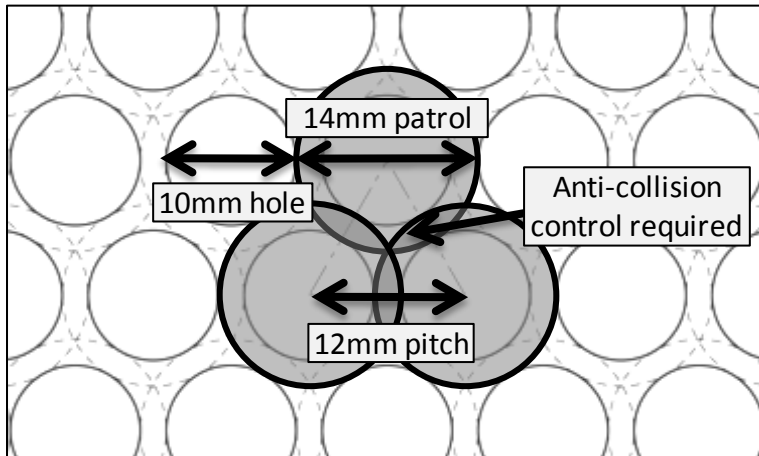


Figure 1. Diagram of hexagonally close packed positioner envelopes. Focal plate has $\varnothing 10\text{mm}$ holes to receive positioners. Spacing is 12mm center-to-center. Positioners must patrol overlapping $\varnothing 14\text{mm}$ regions to cover the field, thus requiring the ability to reach outside the positioner's own mechanical envelope, while simultaneously avoid collision with adjacent positioners.

This paper discusses a new type of positioner developed at Lawrence Berkeley National Laboratory (LBNL), with R- θ kinematics driven by DC brushless servomotors. The R- θ kinematics allow simple and predictable anti-collision control, while the servomotors provide fast, precise, low power mechanical input, with off-the-shelf controllers. Radial kinematics are achieved by an extensible flexure, which doubles as an anti-backlash spring.

2. R- θ VERSUS θ - ϕ AND X-Y KINEMATICS

Three kinematic modes are possible to cover the 2D patrol region of the positioner: eccentric axis θ - ϕ , polar R- θ , and Cartesian X-Y. The eccentric axis and polar systems are illustrated in Figure 2.

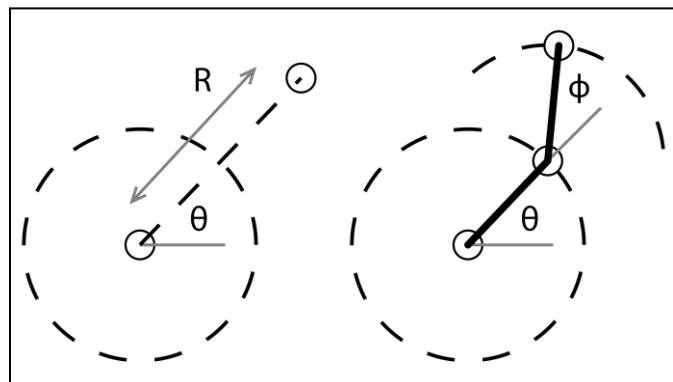


Figure 2. Polar (R- θ) and eccentric axis (θ - ϕ) kinematics.

The eccentric axis system is convenient in that fiber positioners tend to have their motors aligned parallel to the central axis due to the long aspect ratio and tight diameter constraints of the mechanical envelope. It is then relatively simple to provide a pinion gear or offset motor to achieve eccentricity of the ϕ axis. Anti-collision control becomes more challenging, as adjacent positioners must swing the eccentric arm out of each others' way during repositioning if they would otherwise intersect in the overlapping patrol zone. The total time to reposition a field of n positioners increases with the anti-collision complexity, which increases in some relation with n (the authors are unaware of any studies determining the rate of this effect, and at what value of n the field repositioning time might reach an asymptotic limit, if it does). Also, the optical fiber must submit to a combined bend/twist strain as it wraps around the eccentric axis.

An X-Y Cartesian system is unsuitable to a circular patrol region and to the limitations of packaging space: it requires two linear axes, both of which cover a 12mm distance, while not interfering with adjacent positioners at 12mm pitch distance. Echidna achieves something similar with its tip-tilt spine, but at the cost of parasitic tilts at the fiber end which would be unacceptable for BigBOSS injection angle requirements.

A polar kinematic system has a simple repositioning scheme for anti-collision: retract, rotate, extend. The total time to reposition a field of positioners is guaranteed to be constant, no matter the size of the field, and the optical fiber submits to its bending in isolation from its twist, which decouples requirements on fiber testing under mechanical strain. The challenge of a polar kinematic system is in packaging a linear bearing (or analog thereof) for the R axis, given the tight cross-sectional space, and requirement that this linear axis provide extension outside the mechanical envelope into the overlap region.

3. FIBER VIEW CAMERA

The target requirement for precision measurements is positioning error $\leq 40\mu\text{m}$. The BigBOSS corrector includes a fiber view camera, which views the fiber tips of all 5000 positioners on the focal plate through the corrector. Fibers are backlit from the spectrograph side, and the fiber view camera centroids the fiber positions. This closes the positioning control loop, so that after one gross repositioning of all fibers to within the $40\mu\text{m}$ radius circle, the positioners can make final fine steps to target a given location within $5\mu\text{m}$.

4. LBNL R- θ POSITIONER DESIGN

The R- θ positioner developed at LBNL consists of a drive assembly which inserts into a kinematic assembly. The drive assembly has two DC brushless servo motors, and the kinematic assembly contains mechanical features to guide the radial and rotational axes. The rotational axis (θ) is controlled by a bearing cartridge, while the radial axis (R) is controlled by a flexure. The flexure, pulled by a gel-spun UHMW PE cord, retracts into the housing, which provides a natural hard-stop. The spring force of the flexure is arranged to naturally reject gear backlash. The design is diagrammed in Figure 3, with a photograph of a prototype shown in Figure 4.

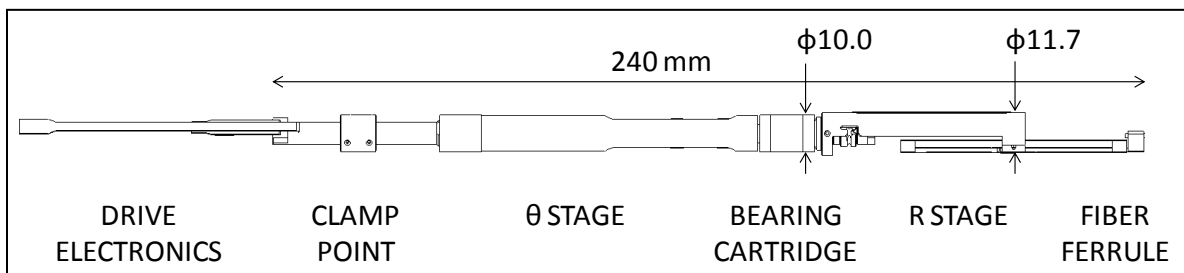


Figure 3. LBNL R- θ positioner design. Drive assembly contains two DC brushless motors and supports the clamp point. It inserts into the θ stage, where it transmits rotation both to the θ and R axes.

At the tip of the flexure, a clamping feature supports the fiber ferrule. Fiber routing throughout the assembly guarantees long lengths over which to bend and to twist the fiber in a gentle manner, without over-constraint. At the base of the drive assembly, each positioner has a drive electronics board, controlling the servo motors.



Figure 4. Prototype R-θ positioner. A marking pen is included in the picture to give scale.

5. SUB-COMPONENT TESTING

During the design and early prototyping phases, extensive testing was performed on key components of the positioner, feeding back improvements to the design in a rapid, iterative manner. A summary of some important results are given in this section.

5.1 Flexure testing

An automated test system was developed using a video coordinate measuring machine, which observes an optical target mounted on the flexure. The target is mounted in the same location where the fiber ferrule is mounted in the full positioner assembly. Mechanical actuation of the flexure was tested with two methods: a lever-driven design and a cord-pulled design, as shown in Figure 5.

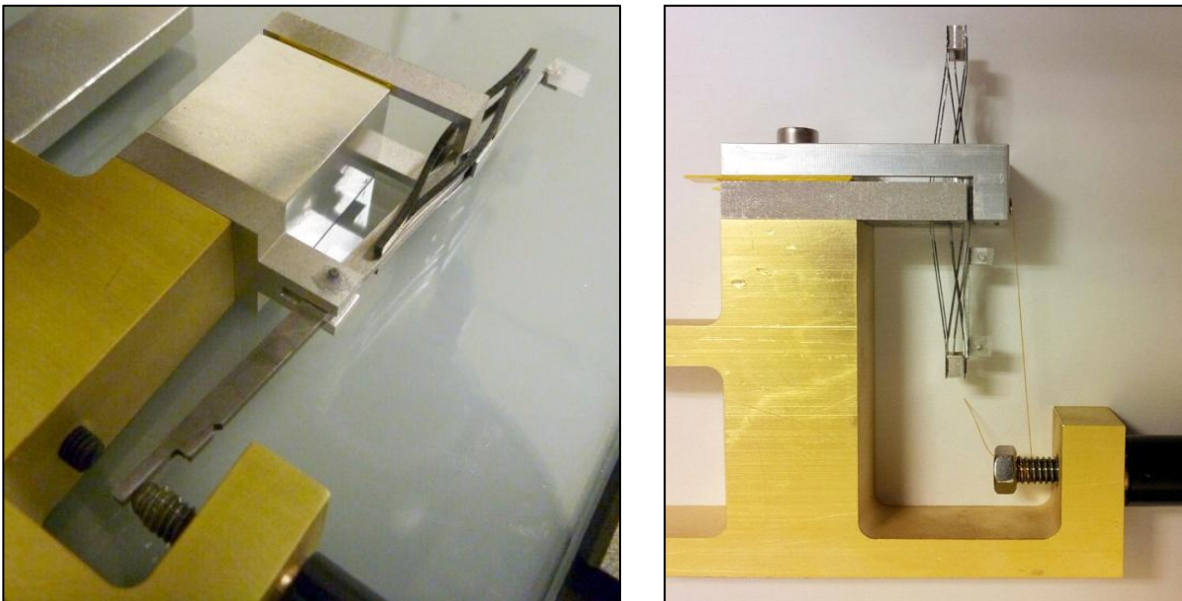


Figure 5. Flexure actuation methods on test stand. *Left:* lever-driven. *Right:* cord-driven.

Several materials were experimented with for flexure construction. An anisotropic fiber-reinforced composite material, designed for high shear stiffness with low bend stiffness, was prototyped but rejected in favor of a precipitation hardened stainless steel. Results from an early test with a composite flexure were conceptually promising, but well outside of required performance, as shown in Figure 6.

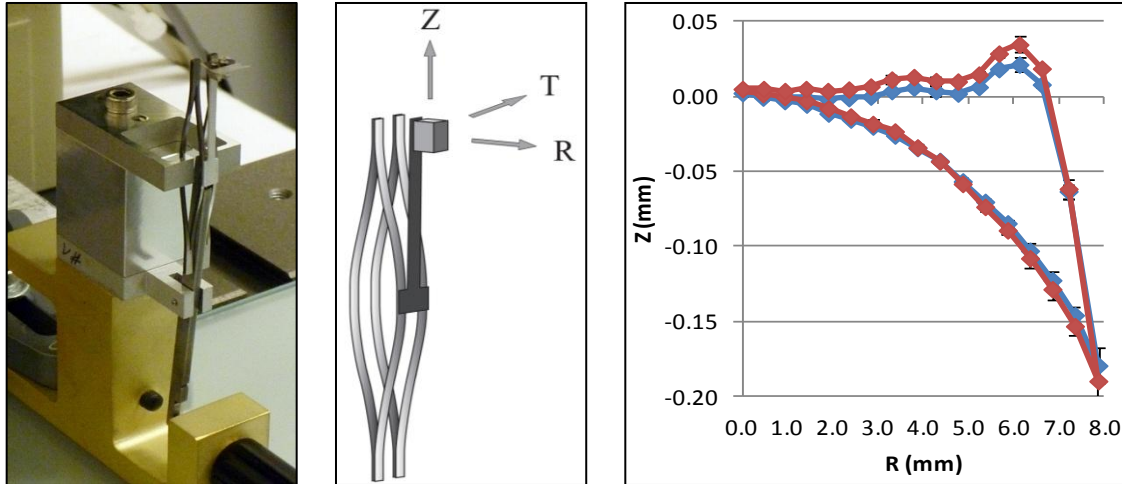


Figure 6. Early fiber-reinforced composite flexure test. *Left*: Flexure on video CMM test stand. *Center*: Coordinate directions of flexure. *Right*: Parasitic defocus error (Z, the axial direction) of this early flexure design, when driven by a lever. Extension stroke drags target downward 200 μ m along a smooth curve; hysteresis peak of return stroke is due to friction reversal at the lever-flexure contact point.

The early testing indicated that control of frictional actuation forces as well as geometry corrections to stabilize internal moments within the flexure were more important than material choice of the leaves. The steel leaf material eventually chosen provides high enough yield strength with the advantage of inexpensive manufacturing controls. Finite element analysis indicated proper proportions of components and leaf thicknesses. Ultimately, an effective combination of parameters was found with minimum sensitivity to manufacturing errors. With adequate control of friction at lever contact surfaces, parasitic defocus error was consistently measured below 30 μ m peak-to-peak. Approaching targets from the retraction direction only, the lever driven actuation had defocus < 10 μ m.

A cord-pulled design also performed well, and has cost advantages for holding alignment tolerances during assembly, as well as reduced hysteresis between the extension and retraction strokes. Test results for a typical cord-actuated flexure are shown in Figure 7 and Figure 8.

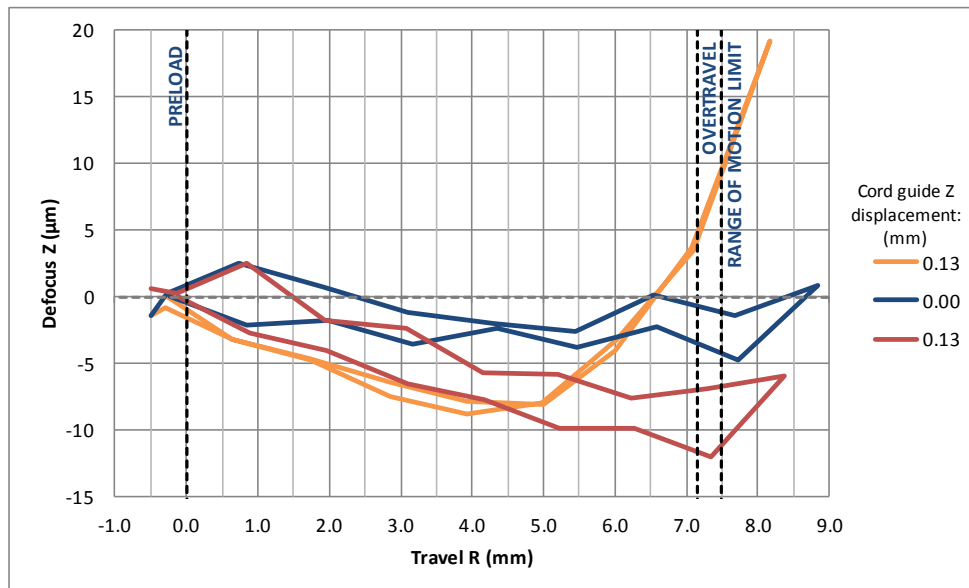


Figure 7. Later flexure design, under cord actuation. At nominal cord angle (relative to the flexure's travel direction), parasitic defocus error is < 5 μ m in both directions of motion. Sensitivity to extreme manufacturing errors (\pm 0.13mm) is shown by two more curves, in which defocus error doubles to ~10 μ m.

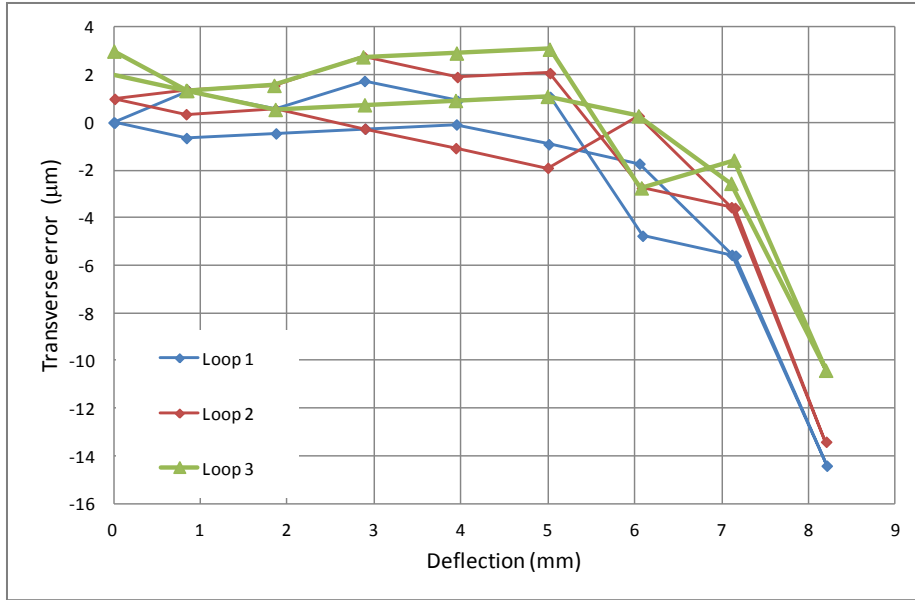


Figure 8. Later flexure design, under cord actuation. Parasitic transverse non-linearity is $< 14\mu\text{m}$ in this test. The test stand lacked cord-angle adjustability in this direction, and with better alignment in the full positioner the non-linearity is lessened. In any event, it is repeatable within an envelope $< 5\mu\text{m}$ peak-to-peak, and therefore easily calibrated out.

5.2 Bearing cartridge testing

Great care was taken in assessment of the bearing cartridge assembly, which controls θ rotation of the upper positioner housing (to which the flexural R-stage is mounted). Furthermore, the outer surface of the bearing cartridge is the mechanical interface to the focal plate. Thus the bearing cartridge controls performance with respect to multiple tight tolerances on positioner tilt, location, and runout. Some views of a typical test setup are given in Figure 9.

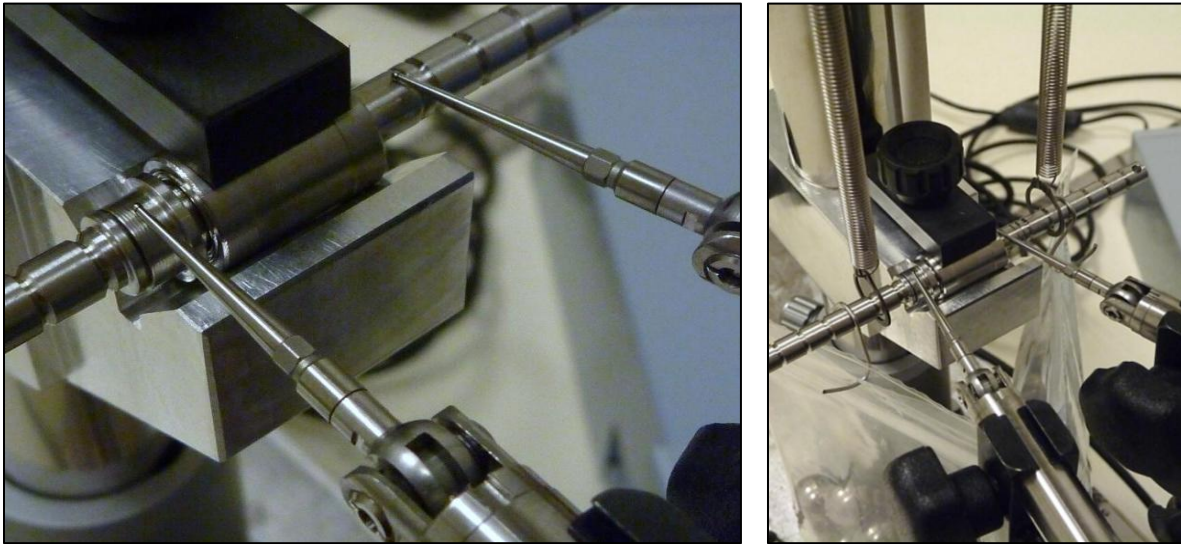


Figure 9. Radial tilt, runout, and stiffness test setups, showing precision force/extension probes.

Tests were made on a sample of 15 bearing cartridges, with results shown in Table 1. Tests were made of radial and axial shaft displacements, tilt errors, and radial and axial stiffness. Results for all displacement and tilt parameters were found to be an order of magnitude or better than strictly necessary to meet science requirements; friction was very low and stiffness high.

Table 1. Bearing cartridge test results. Relevant overall requirement budgets are shown for displacements and tilts.

	Min	Max	Average	Relevant Req't	Unit	Notes
Axial shaft displacement	0.0	1.0	0.4±0.2	20	μm	0.5...3.5 N axial load
Radial shaft displacement	0.8	3.5	2.0±0.7	40	μm	roundness of shaft included
Tilt of nominal shaft axis	0.007	0.032	0.019±0.007	0.15	°	roundness of sleeve included
Tilt due to radial run-out of shaft	0.006	0.018	0.013±0.004	0.15	°	roundness of shaft included
Torque resistance	4.6E-05	5.8E-05	5.0E-05±0.8E-05		°/Nmm	40...120 Nmm load
Axial stiffness			>8		N/μm	-3...+3 N axial load
Radial stiffness			>8		N/μm	-4...+4 N radial load

5.3 Gear train testing

The DC servo motors include a gear reduction head to improve resolution and torque. A gear-train-and-bearing-cartridge assembly was tested for repeatability, with a measurement target at the maximum radial position. The target was rotated away from a nominal point and then returned, and the positional deviation measured to be $< 4\mu\text{m}$ in all cases, with $\sigma = 0.7\mu\text{m}$. Results from this test are plotted in Figure 10.

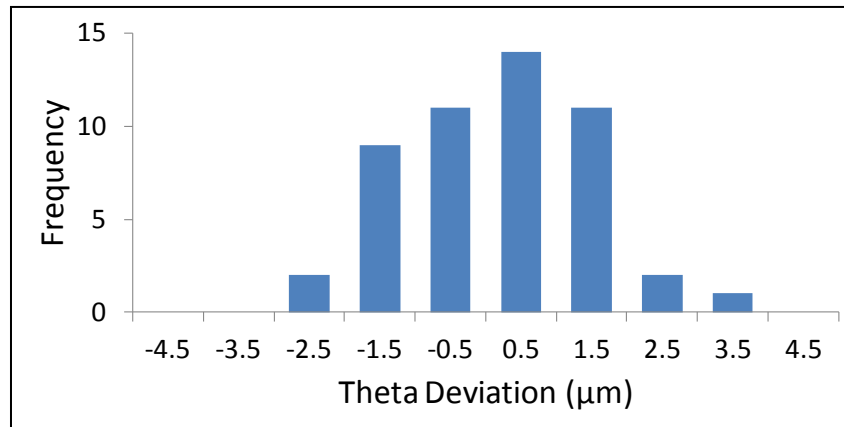


Figure 10. Gear train + bearing repeatability. This plot conveys unidirectional repeatability, not backlash of gears. These deviations are part of the $40\mu\text{m}$ accuracy budget.

5.4 Cord testing

For the cord-actuated flexure, tests were performed to confirm cord strength, durability, and longevity. The test setup for a cyclic endurance test is shown in Figure 11. The UHMW PE cord was cycled repeatedly over representative guide features repeatedly under a tension load equal to the maximum a flexure can provide, and over a displacement distance of $\sim 9\text{mm}$, greater than the R travel of the positioner. In repeated tests, 100k cycles was exceeded before the test was halted, with no occurrence of cord failure. This exceeds the target life by a factor of 5. At a later date, when machined prototype positioner housings became available, the same test was repeated successfully, cycling the cord through the real housing geometry.

In another test, the creep of the cord was assessed, as illustrated in Figure 12. Composed of UHMW PE, the cord is expected to undergo viscoelastic time dependent strain. Under long term constant stress, this strain is presumed to have an elastically recoverable component and a plastic creep component, observed as permanent overall lengthening of the cord. In the test, a constant tensile force equal to the maximum flexure load was applied, and length variations were measured simultaneously with temperature and humidity over a period of 65 days. Strain recovery upon unloading was not measured. The strain rate was found to initially be steep, and then after the first 30 days flattened to a predictable,

linear slope. At this slope, the strain rate is 3.55ppm/day at room temperature. At this rate, during the 5 year BigBOSS observational campaign, the 63mm cord would stretch 0.41mm total, if the flexure were left in its fully-loaded position at all hours. To accommodate this, the positioner design provides 1.8mm of extra wind-up length on its spool, with a simple linear recalibration required at reasonable intervals.

Additionally, six cord samples were tensile tested and found to have an average breaking load of 5.08 lb, with a worst case failure at 3.51 lb. The maximum flexure force is 0.25 lb, thus the minimum factor of safety against tensile failure is 14.

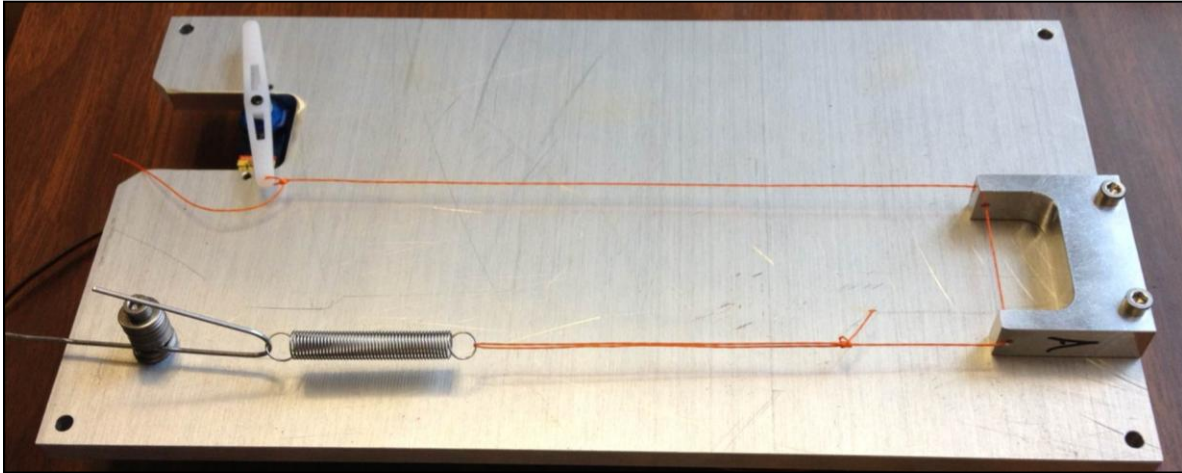


Figure 11. Test stand for cyclic fatigue test of cord. At a nearly constant spring load equal to the maximum flexure force, the cord is repeatedly cycled against representative guide features. Lifetime > 100k cycles is considered success, at which point the test is ended. The test was later repeated with the real geometry of machined prototype housings, prior to assembling the full positioner.



Figure 12. Cord creep test stand. A constant spring force is applied to the cord over several months, while logging length variations on a microscopic scale (increments are 10µm). Temperature and humidity are simultaneously logged, and thermal expansion of the ground plate is accounted for.

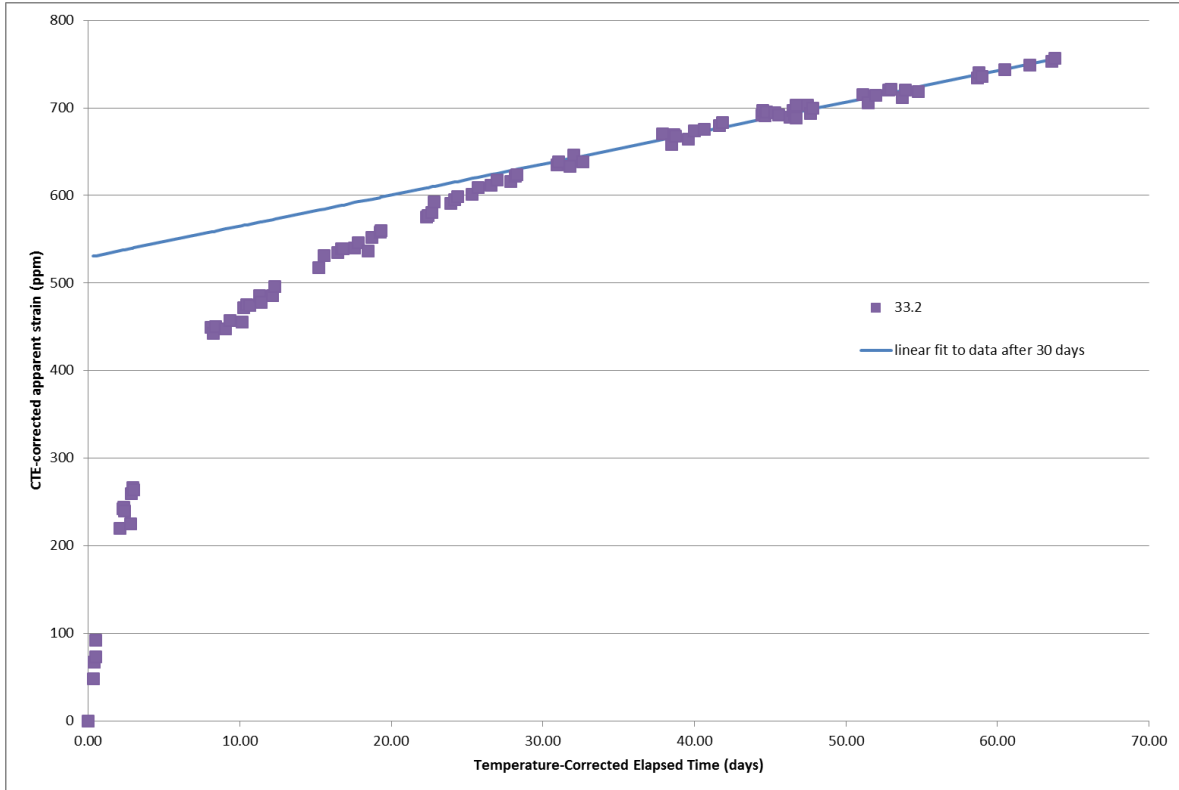


Figure 13. Measured time-dependent strain results for the cord. The strain (in ppm) is plotted against the elapsed time (in days). Strain data is corrected by removing thermal expansion of the ground plate on the test fixture. Time coordinates are slightly adjusted to normalize to a temperature of 297K (logged temperatures during the test varied from a minimum of 291K to a maximum of 303K).

6. FULL POSITIONER TESTING

Testing of the fully-assembled prototype positioner is currently underway as of this writing. A test plan to ascertain resolution, accuracy, power, cooling, and speed has been developed. An initial round of precision measurements have already been made on the first prototype, and are presented below. Repeatability of the R-axis and θ -axis were measured on an automated video CMM in the same manner as the independent flexure tests described above. The test setup is illustrated in Figure 14. An overview showing the test data collected is given in Figure 15.

6.1 R-axis precision

Measurement of the R-axis precision was made with θ held constant. Step positions are relatively large (0.6mm), emulating the gross repositioning phase of the 2 step control loop with the fiber view camera. Repeatability in R was measured to be $\sigma = 6\mu\text{m}$, well within the $40\mu\text{m}$ target. These numbers are for the combined forward and backward data (extending or retracting the flexure), indicating low hysteresis. Furthermore, the worst case error range (maximum error - minimum error) was $34\mu\text{m}$ for combined forward and backward targeting.

If one looks independently at forward data, insisting on approaching a target from that direction only, performance is slightly better: $\sigma = 5\mu\text{m}$ with a max-min envelope of $22\mu\text{m}$. On the other hand, if one only targets in the reverse direction, performance is better still: $\sigma = 3\mu\text{m}$ with a max-min envelope of $12\mu\text{m}$ error. The reason for the poorer performance in the forward direction is believed to be the continuously increasing spring load of the flexure, which continuously increases the stiction force of the cord on its guide. In contrast, in the reverse direction as the flexure unloads the stiction diminishes, and the system is less constrained from adopting a minimum energy configuration. Even so, performance in the forward direction is well within requirements.

Results for the R-axis precision test are plotted in Figure 16.

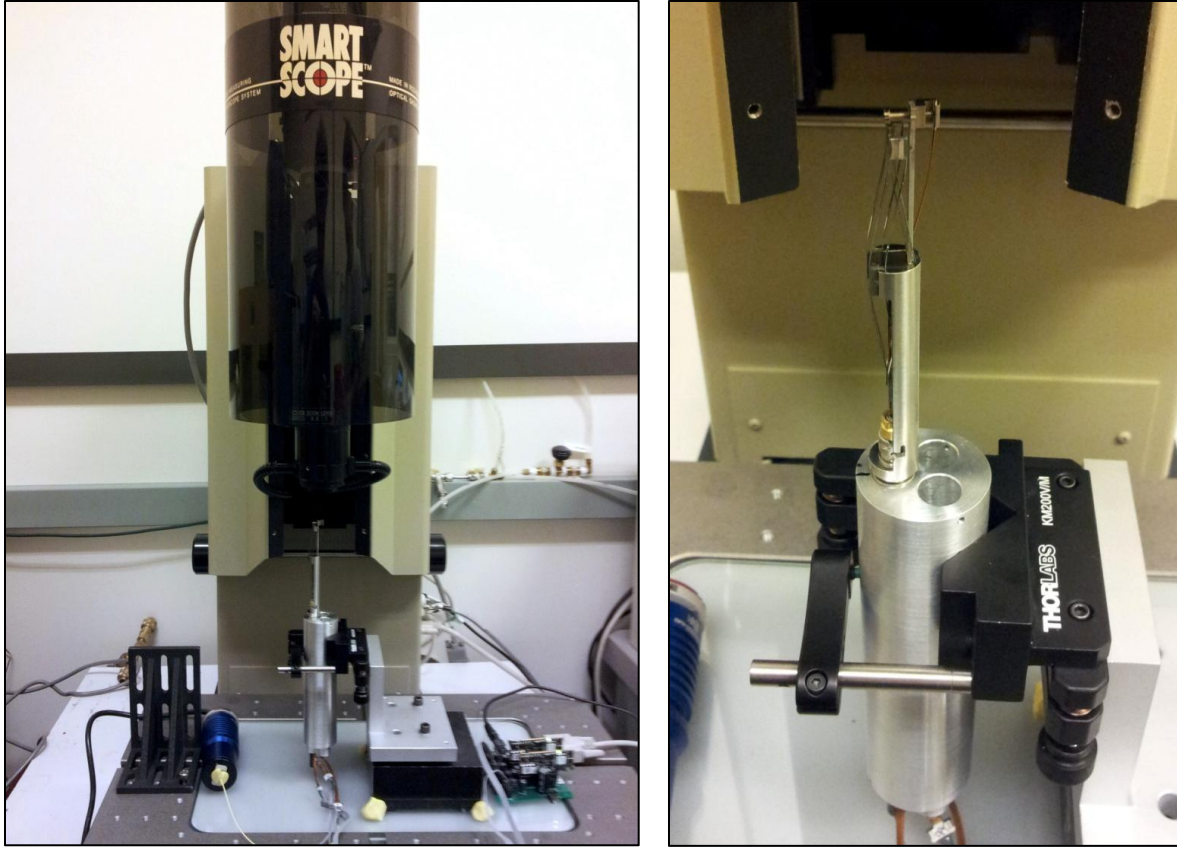


Figure 14. First prototype positioner on test fixture in video coordinate measuring machine.

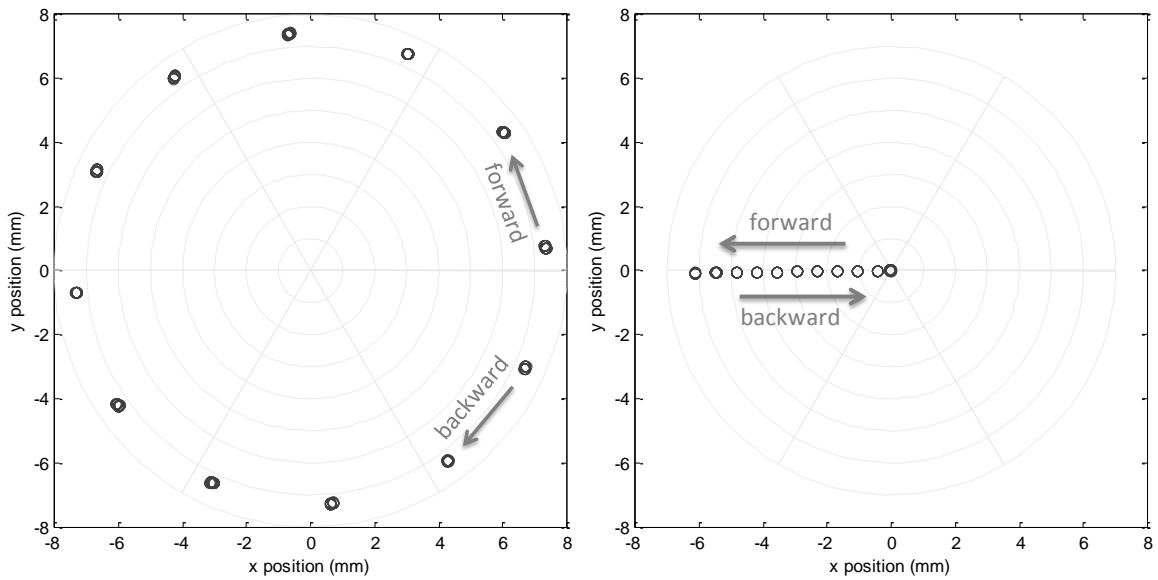


Figure 15. Prototype positioner precision test data. Data recorded on automated video CMM. Ten measurements are made at each target location. *Left*: Circle of target locations at 30° spacing, with R axis held constant. *Right*: Straight line of target points at 0.6mm spacing, with θ axis held constant.

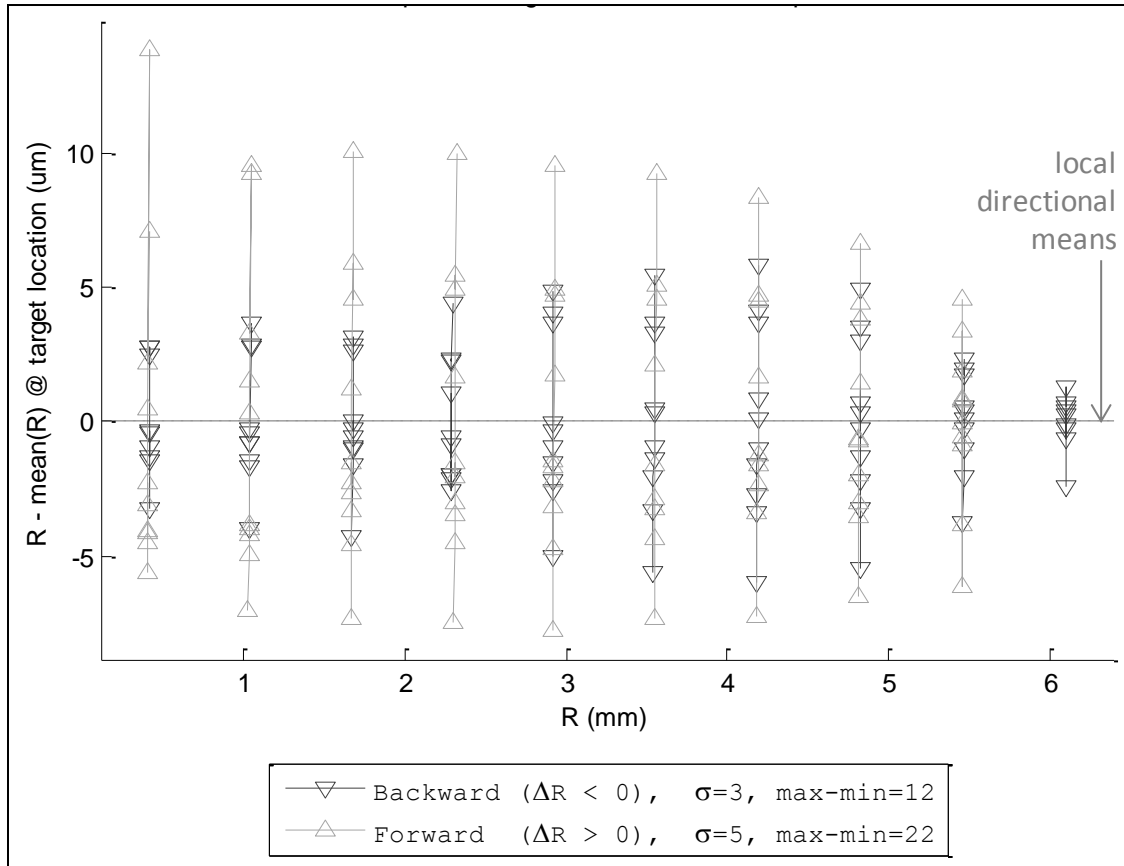


Figure 16. Precision data for R axis. θ is held constant. Performance is given in plot for forward (extension) vs backward (retraction) directions, and found to be very similar. For each target location, the mean of the data at that target, in that direction of motion, establishes the point from which to judge repeatability. If one disregards the direction of motion, and simply combines all forward and backward data into one set, then $\sigma = 6\mu\text{m}$ and maximum - minimum = $34\mu\text{m}$.

6.2 θ -axis precision

Measurement of the θ axis' performance was in turn made with R held constant. Results are plotted in Figure 17, with angular units in degrees. The worst-case projection of these angular errors occurs at maximum radius of 7mm. For both the forward and backward directions, $\sigma = 0.03^\circ$, which projects to $4\mu\text{m}$ error. The maximum - minimum error envelope was again similar for both directions, at 0.17° and 0.16° , projecting to $21\mu\text{m}$ and $20\mu\text{m}$, respectively. These values are all well within the $40\mu\text{m}$ requirement.

If one combines data for the forward and backward directions, gearing backlash becomes evident. In this case, $\sigma = 0.26^\circ$, which projects to $32\mu\text{m}$ at maximum patrol radius, and the max-min error envelope is 0.79° , which projects to $97\mu\text{m}$. A measurement has not yet been made of the gear heads' internal backlash, though the manufacturer claims it is " $\leq 3^\circ$ ". The positioner design takes advantage of the flexure spring force to remove some of the backlash from θ axis, but is more effective at removing backlash in R.

6.3 Repositioning time

A baseline tuning of positioner control parameters was made for the purposes of the precision tests. With these settings, the measured time to rotate the θ -axis 360° is 16 seconds. A full extension-retraction of R is slightly less, 13 seconds. Thus the worst-case total repositioning time for a retract-rotate-extend move is 29 seconds, which is under the 45 second target. A 4x reduction in gear ratio is expected to be possible for future iterations of the prototype, which should cut the repositioning time to under 8 seconds. Also, some further optimization of tuning parameters should improve the speed.

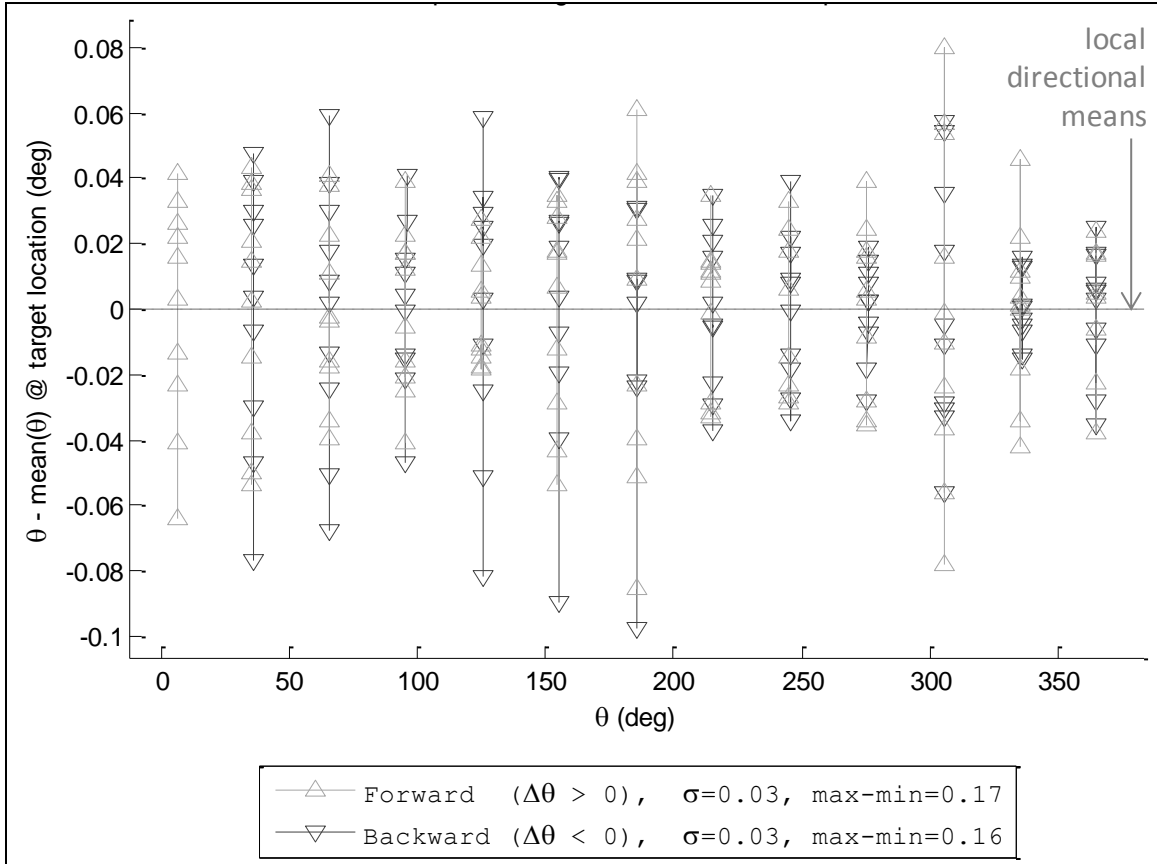


Figure 17. Precision data for θ axis. R is held constant. Performance is given in plot for forward (counter-clockwise) vs backward (clockwise) directions. As with the R motion measurements, performance in forward vs backward directions is found to be very similar. Again, for each target location, the mean of all data at that target in that direction of motion establishes the point from which to judge repeatability. If one treats the data without regard to direction, the combined data set performance is $\sigma = 0.26^\circ$ and maximum - minimum = 0.79° .

7. CONCLUSIONS

The R- θ fiber positioner design developed as a candidate for the BigBOSS instrument has met many tested requirements to date. It is designed for speedy and precise repositioning, with a minimum of complexity in anti-collision control schemes. Manufacturability has been proven through a battery of sub-component testing and ongoing testing of a full prototype. Precision of the R and θ axes have been measured comfortably within the required performance. On the R-axis, backlash is largely eliminated by the natural spring force of its flexural kinematics, while at this point in development, it is preferable to target from one direction when moving along the θ -axis. Flexure actuation has been tested in lever-pushing and cord-pulling configurations; the cord is considered the current baseline for future development. Further work includes the measurement of small step resolution and tilt error, incorporation of hard stops at the limits of travel, measurement of power and cooling requirements, and detailed development of features for fiber ferrule fixation.

ACKNOWLEDGMENTS

We gratefully acknowledge the support of the Director, Office of Science, U.S. Department of Energy, through contract DE-AC03-76SF 00098.

REFERENCES

- [1] J. Edelstein, "Optical fiber systems for the bigboss instrument," *Proc. SPIE 8450-114*, 2012.
- [2] P. Jelinsky, "The bigboss spectrograph," *Proc. SPIE 8446-238*, 2012.
- [3] D. J. Schlegel, C. Bebek, H. Heetderks, S. Ho, M. Lampton, *et al.*, "BigBOSS: The Ground-Based Stage IV Dark Energy Experiment," *arXiv 0904.0468*, 2009.
- [4] D. Schlegel *et al.*, "The BigBOSS Experiment," *arXiv 1106.1706*, 2011.
- [5] N. Mostek, "Mapping the universe with bigboss," *SPIE 8446-24*, 2012.
- [6] H. Hu, X. Xing, C. Zhai, and W. Li, "New type optical fiber positioning unit device for lamost," in *Proceedings of SPIE*, **4837**, pp. 548–555, 2003.
- [7] P. Gillingham, A. Moore, M. Akiyama, J. Brzeski, D. Correll, J. Dawson, T. Farrell, G. Frost, J. Griesbach, R. Haynes, *et al.*, "The fiber multi-object spectrograph(fmos) project- the anglo-australian observatory role," in *Proceedings of SPIE*, **4841**, pp. 985–996, 2003.
- [8] M. Azzaro, S. Becerril, C. Vilar, X. Arrillaga, J. Sanchez, I. Morales, M. Carrera, and F. Prada, "A fiber positioner robot for the gran telescopio canarias," *Arxiv preprint arXiv:1006.0713*, 2010.
- [9] C. Fisher, D. Braun, J. Kaluzny, and T. Haran, "Cobra: A two-degree of freedom fiber optic positioning mechanism," in *Aerospace conference, 2009 IEEE*, pp. 1–11, IEEE, 2009.